Available online at www.sciencedirect.com
ScienceDirect
International Journal of Heat and Mass Transfer 51 (2008) 263–272
International Journal of HEAT and MASS TRANSFER
www.elsevier.com/locate/ijhmt

Heatline method for the visualization of natural convection in a complicated cavity

Amaresh Dalal [a], Manab Kumar Das [b,*]

[a] Department of Mechanical Engineering, Indian Institute of Technology Kanpur, Kanpur 208 016, India
[b] Department of Mechanical Engineering, Indian Institute of Technology Guwahati, Guwahati 781 039, India

Received 4 August 2006; received in revised form 13 March 2007
Available online 18 June 2007

Abstract

In this paper, natural convection inside a two-dimensional cavity with a wavy right vertical wall has been carried out. The bottom wall is heated by a spatially varying temperature and other three walls are kept at constant lower temperature. The integral forms of the governing equations are solved numerically using finite-volume method in non-orthogonal body-fitted coordinate system. SIMPLE algorithm with higher-order upwinding scheme are used. The method of numerical visualization of heat transport for convective heat transfer by heatlines is studied. The heatfunction equation in the transformed plane is solved in terms of dimensionless variables. Results are presented in the form of streamlines, isotherms, heatlines, local and average Nusselt number distribution for a selected range of Rayleigh number (10^0–10^6). The results are presented for three different undulations (1–3) with different wave amplitude (0.00–0.10) and a fluid having Prandtl number 0.71.

Keywords: Natural convection; Numerical simulation; Heatfunction; Laminar flow; Complex geometry

1. Introduction

Streamfunction and streamlines are very convenient and being widely used tool to visualize momentum transport of fluid flow. A less common tool called heatfunction and heatlines approach are used to visualize the transfer of heat by fluid flow. An energy analog concept was first introduced by Kimura and Bejan [1], which provides a better visualization technique for transfer of heat as compared to the traditional isotherms approach.

The method has been followed and extended by several researchers in the following literature [2–10]. These heatline applications are applied to natural convection with simple geometry and boundary conditions. Costa [8,9] dealt with the conjugate heat transfer problem with variable diffusion coefficient and harmonic mean functions. Deng and Tang [10] and Costa [11] have given details about the consistency of the formulations when dealing with conjugate convection/conduction problem. Using streamlines and heatlines method, Deng et al. [12] have studied a two-dimensional, steady state and laminar natural convection in a rectangular enclosure with discrete heat sources on walls. Later on Deng et al. [13] have investigated the characteristics of the airflow and heat/contaminant transport structures in the indoor air environment by means of a convection transport visualization technique. Based on the governing equations, the fluid, heat, and contaminant transport processes are respectively described by the corresponding streamfunction, heatfunction, and massfunction. Numerical results have been presented by the contour function lines, namely, streamlines, heatlines, and masslines. Costa [14] has given a review of

* Corresponding author. Tel.: +91 361 2582655; fax: +91 361 2690762.
E-mail addresses: amaresh@iitk.ac.in (A. Dalal), manab@iitg.ernet.in (Manab Kumar Das).

0017-9310/$ - see front matter © 2007 Elsevier Ltd. All rights reserved.
doi:10.1016/j.ijheatmasstransfer.2007.04.005

Nomenclature

g	gravitational acceleration
H	height of the enclosure
J	Jacobian
L	length of the enclosure
n	number of undulations
Nu	Nusselt number
p	dimensionless pressure
Pr	Prandtl number
P, Q	grid control functions
q_1, q_2, q_3	geometric relations between coordinate systems
Ra	Rayleigh number
S	source term
T	dimensionless temperature
ΔT	differential temperature, dimensionless
U, V	dimensionless contravariant velocity components in ξ and η direction
u, v	dimensionless velocity components in x and y direction
x, y	dimensionless Cartesian coordinates

Greek symbols

α	thermal diffusivity
ξ, η	dimensionless curvilinear coordinates
ϕ	general variable representing u, v and T
λ	wave amplitude
Φ	heatfunction
ψ	streamfunction

Subscripts

av	average
c	cold wall
h	hot wall
l	local
max	maximum
x, y, ξ, η	derivative relative to x, y, ξ, η, respectively

Superscript

*	dimensional form

the Bejan's heatline and massline approach for convection visualization and approach.

Recently, Dalal and Das [15] have studied natural convection in a cavity with one wavy wall of different undulations. The bottom wall was heated by a sinusoidally varying temperature and the other three walls are maintained at cold conditions. In the present work, the heatfunction equation has been modified and solved for a complex geometry. The visualization of the transfer of heat for the convection at Rayleigh number 10^0–10^6 for one-, two- and three-undulations have been done. The amplitude of undulation is varied from 0.00 to 0.10.

2. Governing equations and boundary conditions

The geometry of the two-dimensional square cavity with wavy right vertical wall filled with viscous fluid is shown in Fig. 1. The bottom wall temperature is considered to be spatially varying with sinusoidal temperature distribution. The other three walls are considered to be of constant temperature. The expression of the wavy wall is given by

$$f(y) = 1 - \lambda + \lambda \times \cos(2\pi n y) \tag{1}$$

where n is the number of undulations. Three different cases with one-, two- and three-undulations are studied. The wave amplitude (λ) for three cases is varied from 0.00 to 0.10. The fluid considered in this study is air ($Pr = 0.71$). The Rayleigh number is varied from 10^0 to 10^6.

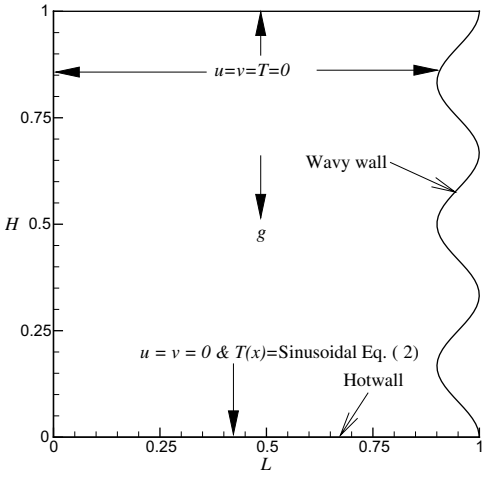

Fig. 1. Flow configuration and boundary condition for three undulations.

The details of the nondimensional governing equations in the physical plane and in the computational plane (ξ, η) are given in [15] along with the boundary conditions.

2.1. Heatfunction equation

To visualize the transfer of heat by fluid flow, an energy analog concept, heatfunction and heatlines, was introduced by Kimura and Bejan [1] which provides a better visualization technique as compared to the traditional isotherm approach. The dimensionless form of heatfunction, Φ, in two-dimension is defined as [1]

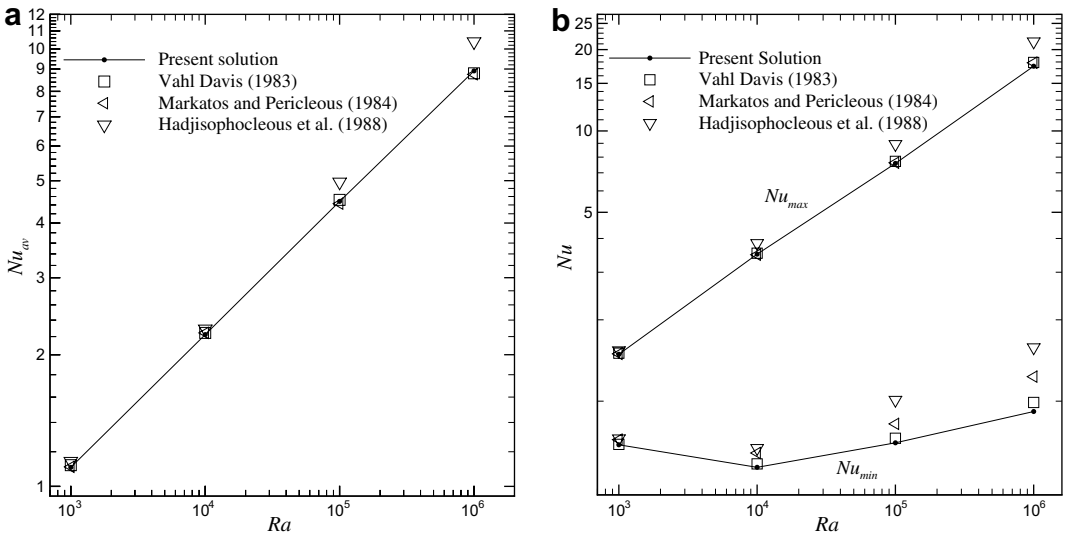

Fig. 2. (a) Comparison of Nu_{av} on hot wall; (b) comparison of Nu_{max} and Nu_{min} on hot wall.

$$\frac{\partial \Phi}{\partial y} = uT - \frac{\partial T}{\partial x} \tag{2}$$

$$-\frac{\partial \Phi}{\partial x} = vT - \frac{\partial T}{\partial y} \tag{3}$$

Eliminating the temperature gradients of the above equations by cross differentiation, a Poisson-type equation is constructed for the heat function.

$$\frac{\partial^2 \Phi}{\partial x^2} + \frac{\partial^2 \Phi}{\partial y^2} = \frac{\partial (uT)}{\partial y} - \frac{\partial (vT)}{\partial x} \tag{4}$$

In the transformed plane (ξ, η), equations of heatfunction take the form

$$\Phi_\eta = UT - \frac{1}{J}\left(q_1 T_\xi - q_2 T_\eta\right) \tag{5}$$

$$-\Phi_\xi = VT - \frac{1}{J}\left(q_3 T_\eta - q_2 T_\xi\right) \tag{6}$$

Eq. (4) is then transformed to computational space

$$\left\{\frac{1}{J}\left(q_1 \Phi_\xi - q_2 \Phi_\eta\right)\right\}_\xi + \left\{\frac{1}{J}\left(-q_2 \Phi_\xi + q_3 \Phi_\eta\right)\right\}_\eta = \left\{-x_\eta (uT)_\xi + x_\xi (uT)_\eta\right\} - \left\{y_\eta (vT)_\xi - y_\xi (vT)_\eta\right\} \tag{7}$$

The boundary conditions for the heatfunction are derived from Eqs. (5) and (6). The left corner of the enclosure is taken as the reference point and its value of heatfunction is taken as zero.

$$\begin{aligned}
&\text{Left wall } \Phi = 0 - \int_0^y \frac{1}{J} q_1 T_\xi \, \mathrm{d}\eta \\
&\text{Top wall } \Phi = \phi(0,1) - \int_0^x \frac{1}{J} q_3 T_\eta \, \mathrm{d}\xi \\
&\text{Right wall } \Phi = \phi(1,0) - \int_0^y \frac{1}{J} q_1 T_\xi \, \mathrm{d}\eta \\
&\text{Bottom wall } \Phi = 0 - \int_0^x \frac{1}{J}\left(q_3 T_\eta - q_2 T_\xi\right) \mathrm{d}\xi
\end{aligned} \tag{8}$$

Eq. (7) is solved for the heatfunction with the boundary conditions given in Eq. (8).

3. Code validation and grid independence study

The governing equations are discretized using staggered, non-uniform control volumes and these equations are solved numerically by finite-volume method. The semi-implicit method or pressure linked equation (SIMPLE) [16] is used to couple momentum and continuity equations. In order to minimize the numerical diffusion errors, the deferred QUICK scheme of Hayase et al. [17] is employed in approximating the convective terms for both

Table 1
Average Nusselt number for $Ra = 10^5$ and $\lambda = 0.05$

Grid size	1 Undulation	2 Undulations	3 Undulations
101 × 101	−0.816965	−0.733817	−0.688565
121 × 121	−0.815491 (0.18%)	−0.735125 (0.18%)	−0.695717 (1.04%)
131 × 131	−0.814386 (0.14%)	−0.735526 (0.05%)	−0.695768 (0.01%)

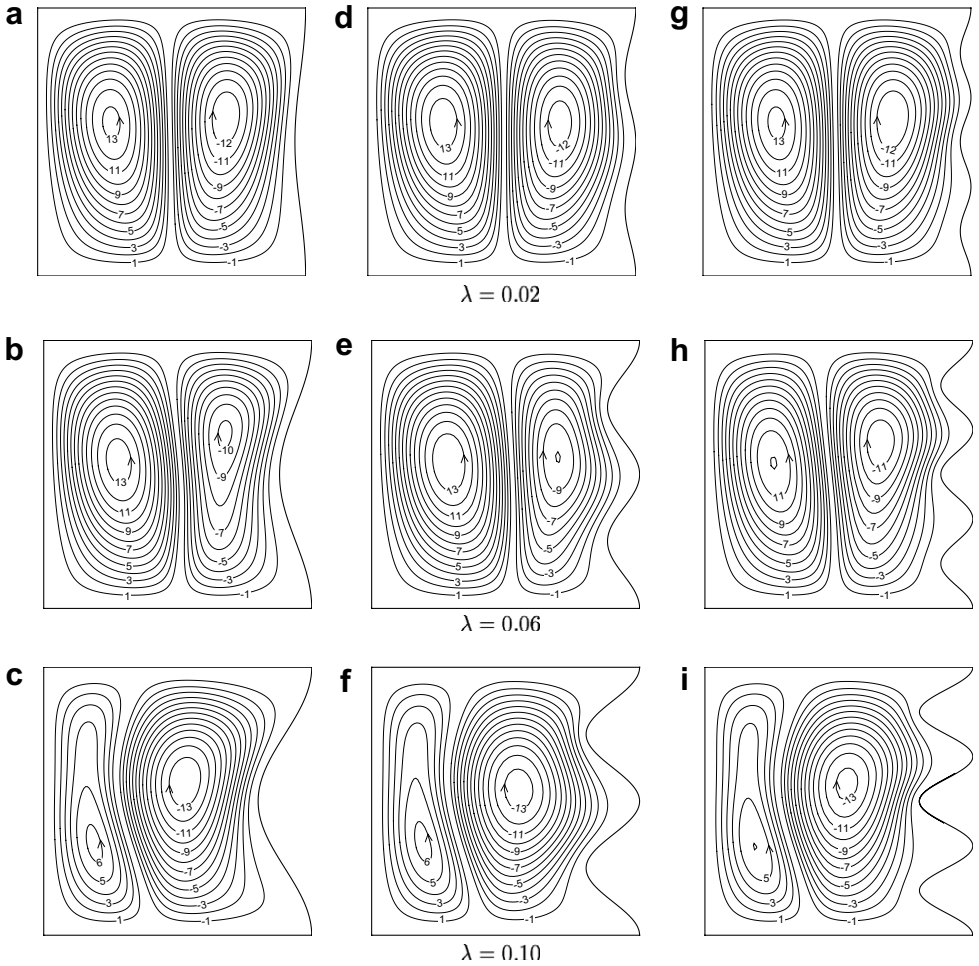

Fig. 3. Streamlines for $Ra = 10^5$.

the momentum equations and energy equation. The central difference scheme is employed near the boundary points for the convective terms. The mass balance for global convergence was taken as 10^{-6}.

The present code is validated with the numerical results of de Vahl Davis [18], Markatos and Perikleous [19] and Hadjisophocleous et al. [20] for the buoyancy driven laminar heat transfer in a square cavity with differentially heated side walls. The left wall is maintained hot while the right wall is cooled. The top and bottom walls are insulated. In the present work, numerical predictions using the developed algorithm, have been obtained for Rayleigh numbers between 10^3 and 10^6 on elliptic mesh with 61×61 grid points. Fig. 2a shows the comparison of average Nusselt number on hot wall. Comparison of maximum and minimum Nusselt number on hot wall is shown in Fig. 2b. Comparison of the results is also given in Dalal and Das [21]. The results are in very good agreement with the benchmark solution. The grid independence test was performed using successively sized grids 101×101, 121×121, and 131×131 for $Ra = 10^5$ and $\lambda = 0.05$. Table 1 shows that for $Ra = 10^5$, there is less change in Nu_{av} on the wavy wall from 121×121 to 131×131 than from

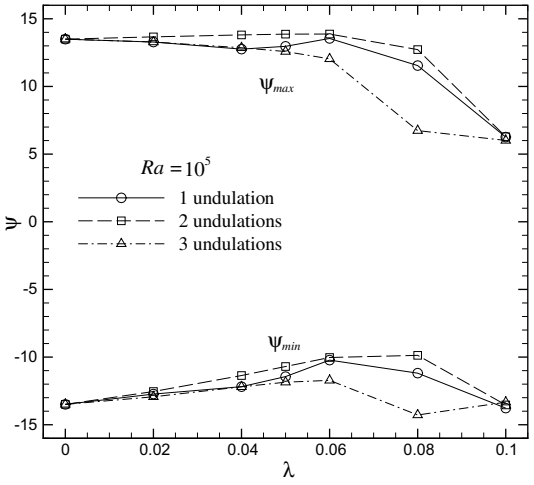

Fig. 4. Maximum and minimum streamfunction distribution for $Ra = 10^5$.

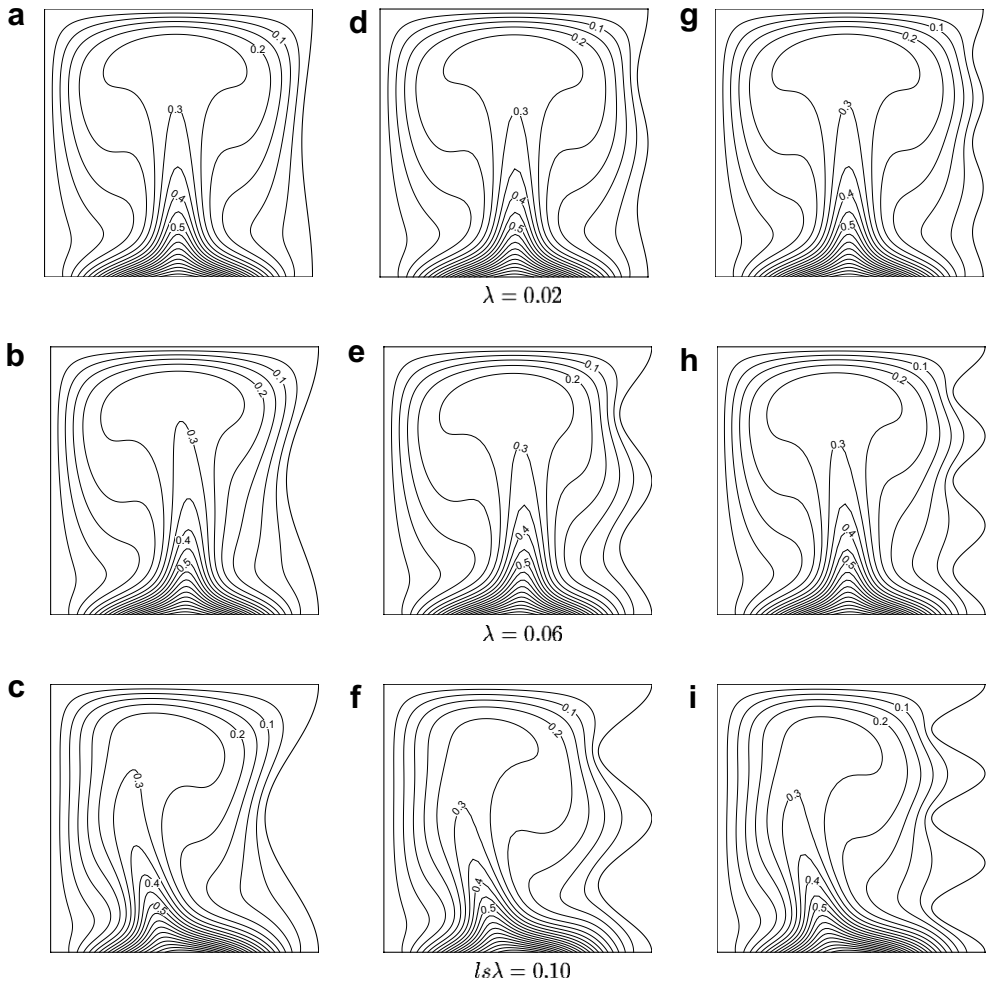

Fig. 5. Isotherms for $Ra = 10^5$.

101 × 101 to 121 × 121. So a grid number of 121 × 121 is chosen for further computation.

4. Results and discussion

A parametric study has been carried out to determine the influence of Rayleigh number on the flow field and effect of number of undulation on heat transfer. The results are for Rayleigh number of 10^0–10^6, Prandtl number of 0.71, and undulation amplitude of 0.00–0.10. The discussion of the following results concerns the streamlines, isotherms, heatlines, local Nusselt number and average Nusselt number distributions on the walls.

4.1. Streamline, isotherm and heatline distribution

4.1.1. Effect of wave amplitude

The streamlines for different amplitude are shown in Fig. 3. As the amplitude is increased to 0.10, the size of the right cell increases and the left cell is squeezed to a rather small fraction of the domain. Because of the direction of motion, the right cell has negative streamfunction values whereas left cell has positive values. Fig. 4 shows the maximum and minimum stream function distribution for $Ra = 10^5$. As λ is increased, for one undulation, the ψ_{max} value (left cell) decreases followed by a temporary rise at around $\lambda = 0.06$ and finally settles to a lower value at $\lambda = 0.1$. For two-undulation case, ψ_{max} remains constant upto $\lambda = 0.06$ and then decreases. For three-undulation case, ψ_{max} continually decreases. The ψ_{min} value (right cell) for one-, two- and three-undulations initially decreases and then is adjusted to nearly the same value as of $\lambda = 0.00$. It is to be noted that the ψ_{max} has same value at $\lambda = 0.1$ for the three-undulations. The same trend is observed for ψ_{min} also.

The isotherms for different amplitude are shown in Fig. 5. Because of the change in the relative size of the cells with λ, the isotherms are observed to have

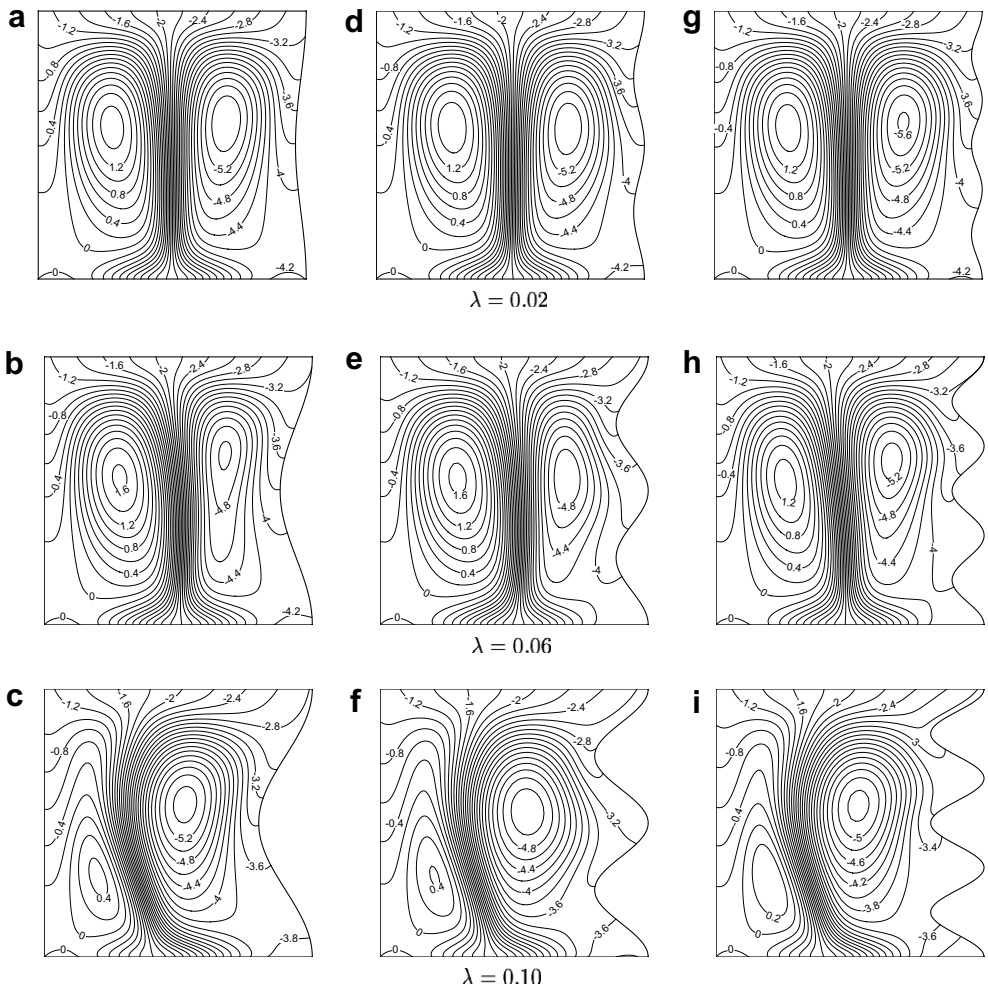

Fig. 6. Heatlines for $Ra = 10^5$.

a skewness towards the left vertical wall as λ is increased.

The heatfunction contours for different undulations and amplitudes are shown in Fig. 6 for $Ra = 10^5$. With the increase in λ, the Φ values are coming down within the domain. For example, on the right wavy wall, the maximum Φ value has come down from -4.2 ($\lambda = 0.02$, Fig. 6g) to -3.8 ($\lambda = 1.0$, Fig. 6i). So the Nu_{av} is decreasing as λ is increased (Table 3 of Dalal and Das [15]).

4.1.2. Effect of Rayleigh number on the heatline distribution

Fig. 7 shows the heatline distribution for one-, two- and three-undulations. The Ra is varied from 10^3 to 10^6 and the amplitude λ is 0.05. As has been discussed by Deng and Tang [10], average Nusselt number Nu_{av} is given by the heatfunction values. To ensure the accuracy of present calculation, the following comparison has been done. For the bottom wall, $Nu_{av} = 1.45$. From heatfunction plot (Fig. 7a), the value of Φ at left corner is 0.0 and at the bottom right corner is -1.4424. So $Nu_{av} = 0.0 - (-1.4424) = 1.4424$. Similarly for the right wall, $Nu_{av} = -0.669581$ (Table 4 of Dalal and Das [15]). From heatfunction computation, the $\Phi = -0.76155$ at the top right corner. So $Nu_{av} = -1.4424 - (-0.76155) = -0.68085$.

It is observed that with the increase of Ra, the magnitude of heatfunction is increasing which implies that the amount of heat transfer is higher (Fig. 7). However, for any particular Ra, it does not change significantly and thus there is no noticeable effect on the heat transfer rate. The heatlines rise as a plume and move in closed vortices as the Ra is increased.

4.2. Heat transfer distribution

The effect of different parameters (i.e., Rayleigh number, undulation and wave amplitude) on heat transfer is described from Nusselt number distribution.

4.2.1. Local heat transfer

The local Nusselt number distributions on left, bottom and top walls are shown in Fig. 8. The Nu_l distribution

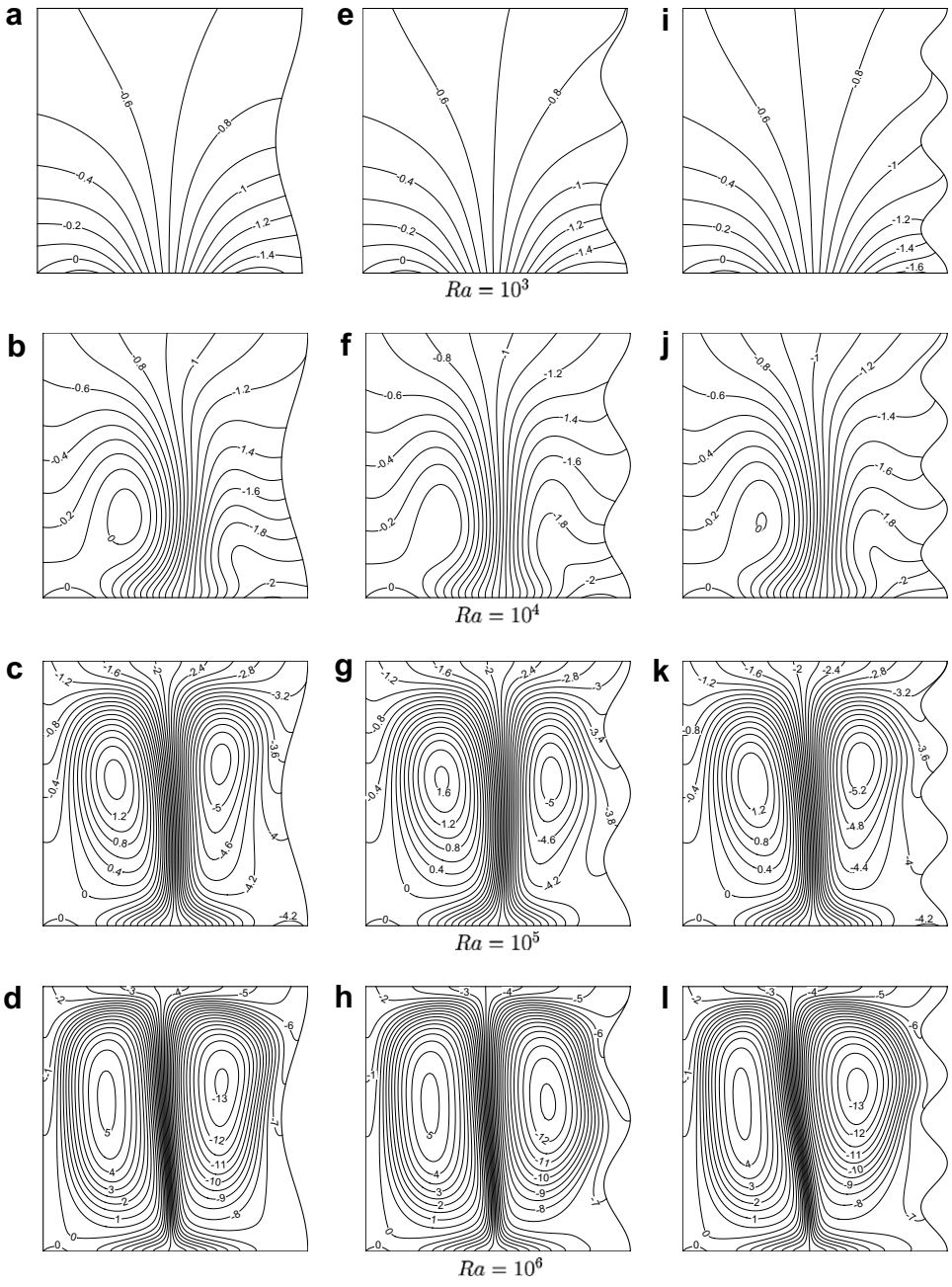

Fig. 7. Heatlines for $\lambda = 0.05$.

on the left wall (Fig. 8a) has similar feature to that of on the wavy wall (Fig. 5a of [15]). For $Ra = 10^3$, the Nu_l distribution on the bottom wall has one maximum location (Fig. 8c) (because of conduction mode of heat transfer). However, as Ra is increased to 10^5 and above, two peaks a little away from $x = 0.5$ are observed because of the sinusoidal boundary condition and thermal boundary layer. For the higher Rayleigh numbers, the recirculation intensity increases and the isothermal lines are concentrated near the middle region of the top wall which produces a peak in the local Nusselt number near the middle region of top wall of the enclosure (Fig. 8e). It is observed that the number of undulation has a minor effect on the Nu_l distribution on the left, bottom and top walls (Fig. 8b, d and f) respectively.

4.2.2. Overall heat transfer

The average Nusselt number distribution on left, bottom and top wall is shown in Fig. 9. Increase in λ and number of undulation has a beneficial effect on the Nu_{av} for the left wall (Fig. 9a–b). However for bottom and top wall, Nu_{av} decreases with the increase of λ and number of undulations (Fig. 9c–f). This is due to the interaction of the convection current with the complex geometry created by undulation.

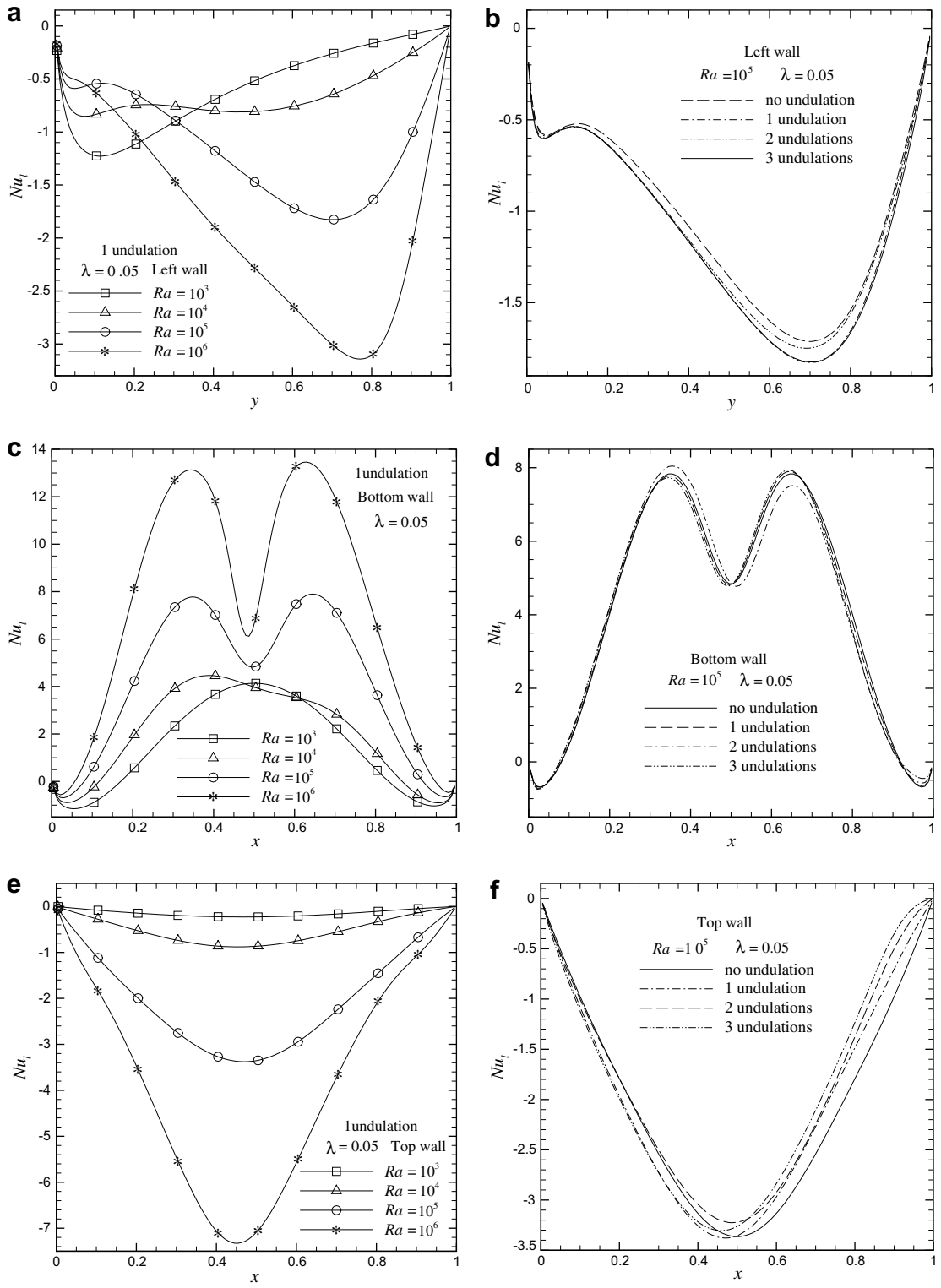

Fig. 8. Local Nusselt number.

5. Concluding remarks

Buoyancy induced flow and heat transfer inside a cavity with sinusoidal temperature boundary condition on the bottom wall and constant cold temperature boundary condition on other three walls is investigated numerically. The heatfunction equations have been numerically solved in a complex geometry formulation. The basic characteristics of heatfunction/heatlines are useful for perceiving the visualization results. The visualization of heatlines exhibit the convection of heat by fluid flow. It has been shown that the level of heatfunction lines are

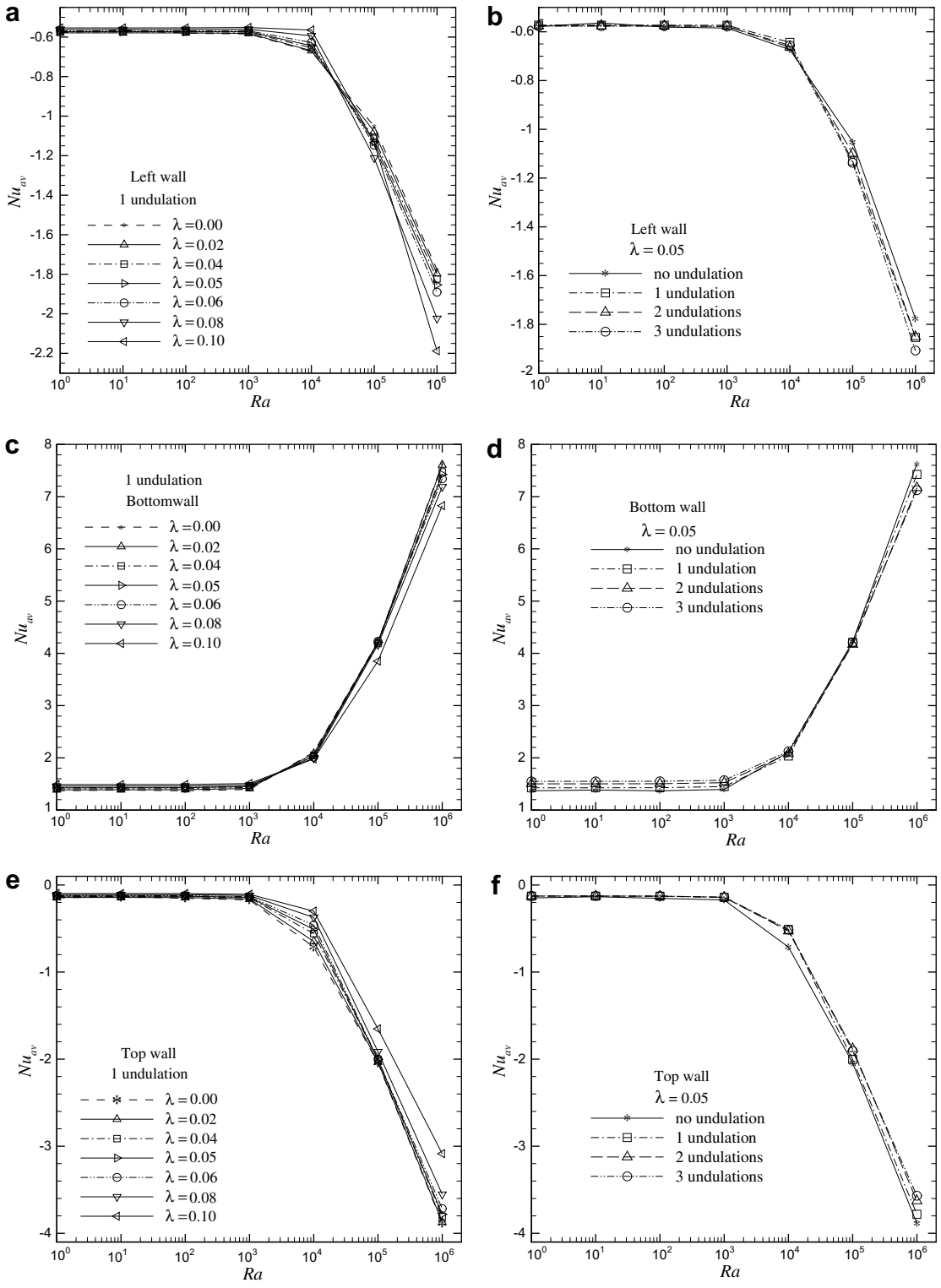

Fig. 9. Average Nusselt number.

a direct measure of the heat transfer and it has been validated by examples.

The heat rejection by the left and the top wall increases with *Ra*. The heat addition by the bottom wall increases with *Ra*. The heat transfer process is slightly affected by the presence of undulations on the right wall.

References

[1] S. Kimura, A. Bejan, The heatline visualization of convective heat transfer, ASME J. Heat Transfer 105 (1983) 916–919.

[2] D. Littlefield, P. Desai, Buoyant laminar convection in a vertical cylindrical annulus, ASME J. Heat Transfer 108 (1986) 814–821.

[3] F.L. Bello-Ochende, A heat function formulation for thermal convection in a square cavity, Comput. Methods Appl. Mech. Eng. 68 (1988) 141–149.
[4] S.K. Aggarwal, A. Manhapra, Use of heatlines for unsteady buoyancy-driven flow in a cylindrical enclosure, ASME J. Heat Transfer 111 (1989) 576–578.
[5] C.J. Ho, Y.H. Lin, Natural convection of cold water in a vertical annulus with constant heat flux on the inner wall, ASME J. Heat Transfer 112 (1990) 117–123.
[6] A.M. Morega, A. Bejan, Heatline visualization of forced convection boundary layers, Int. J. Heat Mass Transfer 36 (1993) 3957–3966.
[7] H.Y. Wang, F. Penot, J.B. Sauliner, Numerical study of a buoyancy-induced flow along a vertical plate with discretely heated integrated circuit packages, Int. J. Heat Mass Transfer 40 (1997) 1509–1520.
[8] V.A.F. Costa, Double diffusive natural convection in a square enclosure with heat and mass diffusive walls, Int. J. Heat Mass Transfer 40 (1997) 4061–4071.
[9] V.A.F. Costa, Unification of the streamline, heatline and massline methods for the visualization of two-dimensional transport phenomena, Int. J. Heat Mass Transfer 42 (1999) 27–33.
[10] Q.-H. Deng, G.-F. Tang, Numerical visualization of mass and heat transport for conjugate natural convection/heat conduction by streamline and heatline, Int. J. Heat Mass Transfer 45 (2002) 2373–2385.
[11] V.A.F. Costa, Comment on the paper by Qi-Hong Deng, Guang-Fa Tang, Numerical visualization of mass and heat transport for conjugate natural convection/heat conduction by streamline and heatline, IJHMT 45 (11) (2002) 2373–2385, Int. J. Heat Mass Transfer 46 (2003) 185–187.
[12] Q.-H. Deng, G.-F. Tang, Y. Li, A combined temperature scale for analyzing natural convection in rectangular enclosures with discrete wall heat sources, Int. J. Heat Mass Transfer 45 (2002) 3437–3446.
[13] Q.-H. Deng, J. Zhou, C. Mei, Y.-M. Shen, Fluid, heat and contaminant transport structures of laminar double-diffusive mixed convection in a two-dimensional ventilated enclosure, Int. J. Heat Mass Transfer 47 (2004) 5257–5269.
[14] V.A.F. Costa, Bejan's heatlines and masslines for convection visualization and analysis, Appl. Mech. Rev. 59 (2006) 126–145.
[15] A. Dalal, M.K. Das, Natural convection in a cavity with a wavy wall heated from below and uniformly cooled from the top and both sides, ASME J. Heat Transfer 128 (2006) 717–725.
[16] S.V. Patankar, Numerical Heat Transfer and Fluid Flow, Hemisphere Publishing Co., Washington, DC, 1980.
[17] T. Hayase, J.A.C. Humphrey, R. Greif, A consistently formulated QUICK scheme for fast and stable convergence using finite-volume iterative calculation procedures, J. Comput. Phys. 98 (1992) 108–118.
[18] G. de Vahl Davis, Natural convection of air in a square cavity: A benchmark numerical solution, Int. J. Numer. Methods Fluids 3 (1983) 249–264.
[19] N.C. Markatos, K.A. Perikleous, Laminar and turbulent natural convection in an enclosed cavity, Int. J. Heat Mass Transfer 27 (1984) 755–772.
[20] G.V. Hadjisophocleous, A.C.M. Sousa, J.E.S. Venart, Prediction of transient natural convection in enclosures of arbitrary geometry using a nonorthogonal numerical model, Numer. Heat Transfer 13 (1988) 373–392.
[21] A. Dalal, M.K. Das, Laminar natural convection in an inclined complicated cavity with spatially variable wall temperature, Int. J. Heat Mass Transfer 48 (2005) 2986–3007.